ARTICLE OPEN

Check for updates

Crossover of high-energy spin fluctuations from collective triplons to localized magnetic excitations in $Sr_{14-x}Ca_xCu_{24}O_{41}$ ladders

Y. Tseng[1,2✉], J. Thomas[3], W. Zhang[1], E. Paris[1], P. Puphal[4], R. Bag[5], G. Deng[6], T. C. Asmara[1], V. N. Strocov[1], S. Singh[5], E. Pomjakushina[4], U. Kumar[3], A. Nocera[7], H. M. Rønnow[2], S. Johnston[3✉] and T. Schmitt[1✉]

We studied the magnetic excitations in the quasi-one-dimensional (q-1D) ladder subsystem of $Sr_{14-x}Ca_xCu_{24}O_{41}$ (SCCO) using Cu L_3-edge resonant inelastic X-ray scattering (RIXS). By comparing momentum-resolved RIXS spectra with high ($x = 12.2$) and without ($x = 0$) Ca content, we track the evolution of the magnetic excitations from collective two-triplon (2 T) excitations ($x = 0$) to weakly-dispersive gapped modes at an energy of 280 meV ($x = 12.2$). Density matrix renormalization group (DMRG) calculations of the RIXS response in the doped ladders suggest that the flat magnetic dispersion and damped excitation profile observed at $x = 12.2$ originates from enhanced hole localization. This interpretation is supported by polarization-dependent RIXS measurements, where we disentangle the spin-conserving $\Delta S = 0$ scattering from the predominant $\Delta S = 1$ spin-flip signal in the RIXS spectra. The results show that the low-energy weight in the $\Delta S = 0$ channel is depleted when Sr is replaced by Ca, consistent with a reduced carrier mobility. Our results demonstrate that off-ladder impurities can affect both the low-energy magnetic excitations and superconducting correlations in the CuO_4 plaquettes. Finally, our study characterizes the magnetic and charge fluctuations in the phase from which superconductivity emerges in SCCO at elevated pressures.

npj Quantum Materials (2022)7:92 ; https://doi.org/10.1038/s41535-022-00502-1

INTRODUCTION

Antiferromagnetic spin fluctuations are a promising candidate for mediating high-temperature superconductivity (HTSC) in cuprates[1]; however, the precise relationship between magnetism and superconductivity (SC) across the cuprate phase diagram remains unclear despite extensive studies. This uncertainty is due, in part, to the fact that modeling the competition between local moment formation and itinerant quasiparticles with doping is a tremendously difficult problem.

The quasi-one-dimensional (q-1D) spin ladders (Fig. 1) serve as an ideal platform to tackle this issue. Doped cuprate ladders share several similarities with two-dimensional (2D) cuprates, including high-energy spin-fluctuations[2], d-wave pairing[3–5], non-Fermi-liquid transport behavior[6], and large magnetic exchange couplings[7]. A SC phase has also been observed at elevated pressure (1.5–8 GPa) in the hybrid chain-ladder materials $Sr_{14-x}Ca_xCu_{24}O_{41}$ (SCCO) for $11 < x < 14$[8–10]. Importantly, q-1D spin ladders are also more amenable to modeling[3–5]. Characterizing the magnetic excitations in these materials will, therefore, help us better understand HTSC in cuprates.

Magnetic excitations in even-leg ladders can be viewed as coupled spinons, i.e. triplons, due to the exchange interactions across their rungs (Fig. 1b)[3–5]. In the undoped ladders, these triplon excitations are gapped[3–5,11,12], and their spectra near the zone-boundary closely resemble the prototypical magnon-like excitations observed in 2D SC cuprates[13–15]. Conversely, experimental studies of triplons in doped ladders are sparse. Inelastic neutron scattering (INS) experiments discovered that the one-triplon gap at $\mathbf{q} \equiv (q_{\text{leg}}, q_{\text{rung}}) = (\pi, \pi)$ survives up to $x = 12.2$ in SCCO, and is nearly unchanged compared to $x = 0$[16,17]. Nuclear magnetic resonance (NMR) studies on SCCO, on the other hand, find that the triplon gap decreases with increasing Ca content, which develops into a gap collapse at elevated pressure[18–20]. Although dispersing one- and two-triplon excitations have been reported in the nearly undoped ladder $Sr_{10}La_4Cu_{24}O_{41}$ using INS[12], comprehensive studies of their corresponding doping-dependence are lacking. While these studies have provided some insight into the doping-driven changes in the magnetic excitations of ladder systems, a systematic assessment of the triplon response across a large portion of Brillouin zone as a function of doping has yet to be carried out.

Owing to the strong spin-orbit coupling (SOC) in Cu 2*p* core-levels, Cu L_3-edge resonant inelastic X-ray scattering (RIXS) studies on cuprate materials can probe the momentum-dependent magnetic excitations in the dominant spin-flip channel ($\Delta S = 1$)[21,22]. Due to an order of magnitude difference in the magnetic exchange of the ladder (100 meV) and chain (10 meV) subsystems, a previous Cu L_3-edge RIXS study on $Sr_{14}Cu_{24}O_{41}$ (Sr14) showed that the high-energy magnetic excitations at around 100–350 meV are dominated by the ladder triplons when probed at the Cu $3d^9$ resonance[23].

In this letter, we present a Cu L_3-edge RIXS study of the ladders in SCCO with varied Ca content ($x = 0$ and $x = 12.2$). Since superconductivity occurs in SCCO samples with $11 < x < 14$ under

[1]Photon Science Division, Paul Scherrer Institut, CH-5232 Villigen PSI, Switzerland. [2]Laboratory for Quantum Magnetism, Institute of Physics, École Polytechnique Fédérale de Lausanne (EPFL), Vaud, Switzerland. [3]Department of Physics and Astronomy, The University of Tennessee, Knoxville, TN 37996, USA. [4]Laboratory for Multiscale Materials Experiments, Paul Scherrer Institut, Villigen CH-5232, Switzerland. [5]Indian Institute of Science Education and Research, Dr. Homi Bhabha Road, Pune, Maharashtra 411008, India. [6]Australian Centre for Neutron Scattering, Australian Nuclear Science and Technology Organisation, New Illawarra Road, Lucas Heights, NSW 2234, Australia. [7]Department of Physics and Astronomy and Stewart Blusson Quantum Matter Institute, University of British Columbia, Vancouver, BC V6T 1Z1, Canada. ✉email: tsengy@mit.edu; sjohn145@utk.edu; thorsten.schmitt@psi.ch

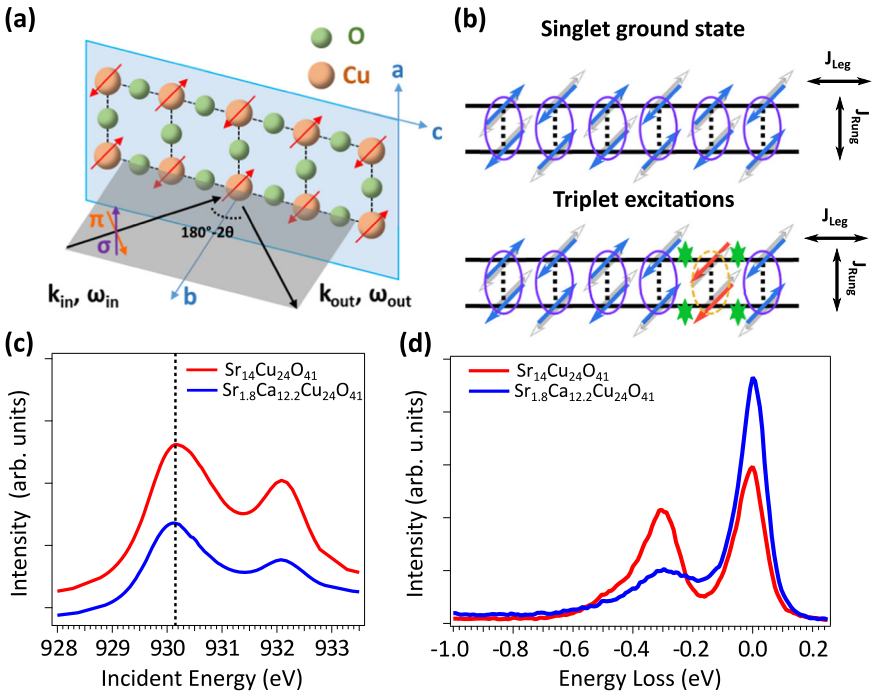

Fig. 1 Experimental overview and schematic of ladder triplon excitations. Schematics of (**a**) RIXS experimental geometry with the orientation of the two-leg Cu_2O_3 ladders in SCCO. The ladder-leg direction is along *c*-axis, with lattice constant c_{leg} ~3.9 Å. **b** $S = 1$ triplon excitations (orange dashed-line ellipse) in two-leg quantum spin ladders. The local antiferromagnetic interactions along the ladder leg and rung are mediated by spins (blue arrows) with equal probability pointing along any directions (opposite direction denoted as gray hollow arrows). The rung-singlets (purple ellipses) interact through ladder-leg exchange coupling. **c** Main resonances of Cu L_3-edge XAS. $3d^9$ white line is marked by the black dashed-line. **d** Cu L_3-edge RIXS spectra taken at $3d^9$ peak at $q_{leg} = -0.31$ (rlu) in σ polarization. Here, a negative (positive) momentum transfer indicates the RIXS data taken in grazing incidence (emission) geometry.

hydrostatic pressure[8–10], our measurements contrast the magnetic excitations of non-superconducting and superconducting samples. We observe a clear evolution in the low-energy RIXS spectra from collective two-triplon excitations to weakly-dispersive excitations as Sr is replaced by Ca. By comparing with numerical calculations of different disordered Hubbard ladder models, we find that the evolution of the spin excitations is consistent with hole-localization induced by off-ladder impurities. This conclusion is supported by a polarization analysis that uncovers spectral depletion of the charge-like excitations probed in the spin-conserving $\Delta S = 0$ scattering channel, reflective of suppressed carrier mobility. Our results naturally explain the observation of low-temperature insulating phases for high Ca content at ambient pressure, despite the expected increase of ladder holes[6,8,9]. Since SCCO serves as a bridge between q-1D and 2D cuprates, our study also helps elucidate the interplay between spin fluctuations, chemical pressure (i.e. Ca doping), electronic correlations, and SC in cuprate materials.

RESULTS

Overview of RIXS spectra

Figure 1d shows the Cu L_3-edge RIXS spectra at $q_{leg} = -0.31$ (rlu), where magnetic excitations appear around 200–400 meV. These magnetic excitations have reduced spectral weight and increased broadening when Sr is replaced by Ca. Both RIXS spectra are taken at the $3d^9$ main resonance close to 930 eV indicated in Fig. 1c. (The high-energy inelastic structures, including the local crystal-field splitting of the Cu 3*d* orbitals [dd excitations] from −1.5 to −3 eV loss, and the broad charge-transfer excitations around −4 eV loss and above, are shown in Supplementary Figure 1)

Figures 2a and d display the momentum-dependent RIXS spectra along $\mathbf{q} = (q_{leg}, q_{rung} = 0)$. For Sr14 (Fig. 2a), we observe magnetic excitations corresponding to collective two-triplon excitations with a band minimum at the zone center, in accordance with the previous Cu L_3-edge work[23]. The excitations are broadened in $Sr_{1.8}Ca_{12.2}Cu_{24}O_{41}$ (Sr1.8Ca12.2) (Fig. 2d) and exhibit a flattened dispersion centered around 280 meV loss that extends across a large portion of the Brillouin zone.

Quantifying the carrier concentrations

Before proceeding to an analysis of the data, we first establish the effective doping level of the ladder subsystem as this will play a crucial role in the subsequent modeling. Despite extensive studies, the precise experimental quantification of hole doping and carrier mobility with respect to the Ca content remains challenging in the cuprate ladders. Early experiments on SCCO observed an increase in the low-energy Drude-like weight and enhanced metallicity in samples with elevated Ca content, which led to a speculated hole transfer between the chains and ladders upon isovalent Sr-Ca substitution[24–26]. This transfer was rationalized in a ladder-dominant picture of the transport in SCCO due to the 180° Cu-O-Cu bond angle in the ladders[24–26]. Ca also has a smaller atomic radius, which induces local structural changes in the Cu-O-Cu bond distances and can generate interactions between the chain and ladder subsystems[27]. Recent studies of Sr14, however, revealed that errors up to a factor of 2–5 can occur when quantifying the ladder hole content if charge and magnetic correlations in the chains are not taken into consideration[28].

Given these uncertainties, we estimated the nominal ladder hole densities in Sr14 and Sr1.8Ca12.2 using polarization-dependent O *K*-edge XAS measurements. This procedure is facilitated by the atomic sensitivity of XAS to the distinct Cu-O bonding environments in the edge-sharing CuO_2 chain and two-leg Cu_2O_3 ladder subsystems[29]. By aligning the linearly polarized light vector parallel to the rung or leg direction, the XAS data can

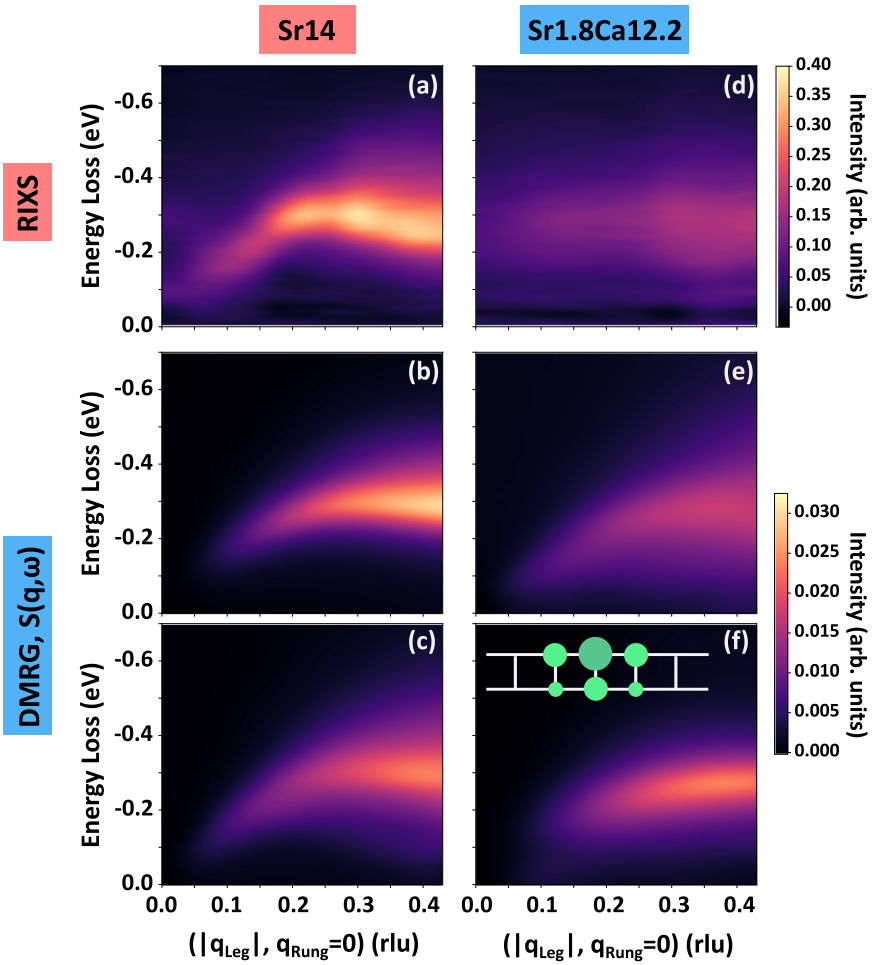

Fig. 2 Experimental and theoretical RIXS spectra with Ca-doping effects. a–c (d–f) Cu L_3-edge RIXS results for Sr14 (Sr1.8Ca12.2). The elastic line in each of the experimental spectra is subtracted for clarity. **a**, **d** Momentum-dependent RIXS experimental spectra for Sr14 and Sr1.8Ca12.2 in σ polarization with bicubic interpolation. **b** Calculated $\Delta S = 1$ RIXS spectra on an undoped ladder cluster for Sr14. **c**, **e** Calculated $\Delta S = 1$ RIXS spectra on doped ladder clusters with hole doping p close to the experimentally determined values from O K-edge XAS results, which are about 6% and 11% for Sr14 and Sr1.8Ca12.2, respectively. The following set of parameters are applied for Sr14 (Sr1.8Ca12.2) on a 32×2 site cluster with spectral convergence: $t_{leg} = 340$ meV, $U = 8t_{leg}$, and $r = 0.85$ ($t_{leg} = 300$ meV, $U = 9t_{leg}$ and $r = 1.1457$). **f** Calculated $\Delta S = 1$ RIXS spectra for Sr1.8Ca12 on a 16×2 site doped ladder cluster with an impurity potential $V_{imp} = 0.5\,U$. We make additional assumptions that the on-site impurities (green circles) are screened poorly, and their potential extends to neighboring sites with strength (diameter size) scaled as $\propto 1/r$. The same t_{leg}, U and r parameters as in (**e**) are adapted in (**f**), with a hole doping of 12.5%.

be used to extract the respective O 2p hole character of the chain and ladder hole subsystems by linear dichroism in Sr14 ($H1$ and $H2$ of 527.5 and 528.2 eV, respectively, in Fig. 3a, b, see caption)[28–31]. To extend this analysis to the Ca-doped compounds, it was assumed that the isovalent Sr-Ca substitution would not alter the total number of doped holes, but rather exchanges the respective weight of chain ($H1$) and ladder ($H2$) hole-doping levels[29] due to the chain-ladder charge transfer inferred in optical and transport experiments[24–26]. Therefore, one can extract the chain and ladder hole concentration by measuring their relative hole peak fraction $H1$ or $H2$ to the total weight of holes $H1+H2$ using polarization-resolved O K-edge XAS (see Supplementary Note 2). Using the model in ref. [29], we obtain excess ladder hole concentrations of 0.06 and 0.11 (holes per Cu atom) for Sr14 and Sr1.8Ca12.2, respectively, in line with previous literature (see Supplementary Note 2).

Localized magnetic excitations due to off-ladder plane impurities

To better understand our experimental results, we modeled the low-energy RIXS response to lowest order in the ultrashort core-hole lifetime expansion[32–34] using density matrix renormalization group (DMRG) calculations for doped Hubbard ladders[35,36]. This approximation has proven accurate for Cu L-edge measurements on $3d^9$ layered 2D cuprates and strongly correlated ladders[33,37]. For Sr14, we adopted parameters resulting in magnetic exchange parameters close to the isotropic limit with $r = J_{rung}/J_{leg} = 0.85$[37]. For Sr1.8Ca12.2, we estimated $r \approx 1.15$ for the highest Ca concentrations using perturbation theory and the available structural data (see Supplementary Fig. 13 and full description in Supplementary Note 3).

Figure 2 compares the experimental Cu L_3-edge RIXS data with DMRG calculations of the dynamical spin structure factor. Here, we consider both undoped and "nominally" doped ladders, as determined by our O K-edge XAS results. As in previous studies, the $\Delta S = 1$ scattering channel dominates the spectra[21]. The RIXS spectra for Sr14 are reasonably well described by both the undoped (Fig. 2b) and doped (Fig. 2c) models; however, we observe a slight increase in the broadening of the two-triplon excitations towards the zone boundary in the 6 % hole-doped ladders, which may be caused by the mixing with charge or Stoner-like continuum excitations like in 2D cuprates[38,39]. Overall, the experimental Sr14 Cu L_3-edge RIXS spectra are better

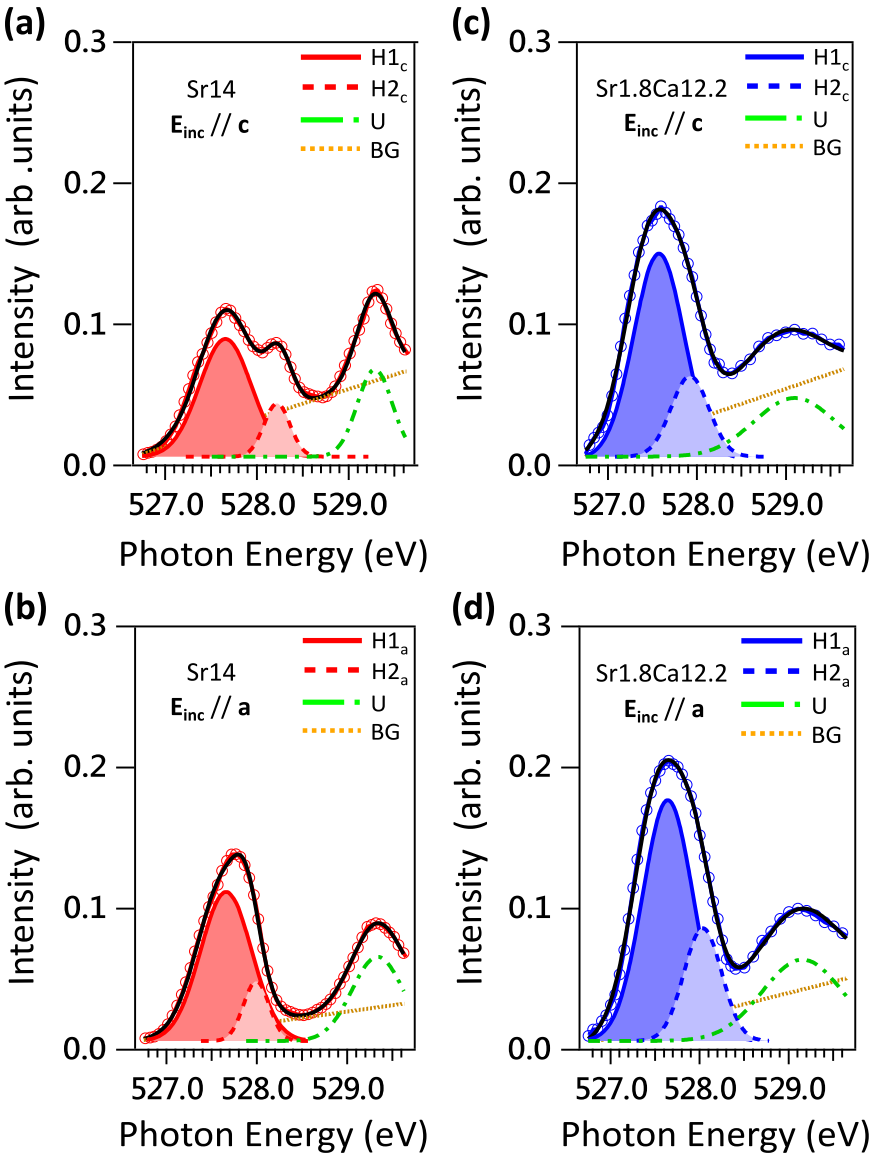

Fig. 3 Evaluated ladder hole concentration with Ca-doping effects. O *K*-edge XAS spectra with fitting components for (**a**–**b**) Sr14 and (**c**–**d**) Sr1.8Ca12.2. A linear background (*BG*) is applied in the spectral fitting. The spectral weight at 527.5, 528.2 and 529.25 eV, respectively, represent the chain hole content *H*1, the ladder hole content *H*2, and the upper Hubbard band[28,29,31]. The polarization of incident X-rays is parallel to the leg c-direction in (**a**, **c**), whereas (**b**, **d**) are measured in the rung a-direction configuration.

described by the DMRG calculation of the 6% nominally doped ladder.

The spin excitations for an 11% hole-doped ladder in Fig. 2e are more diffused compared to the undoped ladder calculations for Sr14 in Fig. 2b, consistent with experiments. However, the increased hole doping also produces a pronounced downturn in the calculated dispersion close to the zone center, which does not occur in our experimental data for Sr1.8Ca12.2. Despite residual low-energy weight, the overall magnetic excitations for Sr1.8Ca12.2 (Fig. 2d) are clearly gapped and relatively dispersionless.

Our perturbation theory analysis in the Supplementary Note 3 indicate that $r \approx 1.15$ for the Ca-doped samples. This estimate explicitly rules out large values of the rung coupling which would produce a flattened magnetic excitation spectrum. Another mechanism must therefore be responsible for the large change in magnetic excitations. Early transport studies found that the resistivity for SCCO with $x > 11$ decreased linearly down to 100–150 K, followed by an abrupt upturn with further cooling[8,9]. The onset of this insulating behavior was attributed to carrier localization at low temperature[9]. We, therefore, consider the effects of localization on the low-energy excitations in Sr1.8Ca12.2. To this end, we performed DMRG calculations on ladders with additional impurity potentials distributed randomly throughout the ladder. The physical picture is that Ca doping introduces impurity potentials outside the ladder planes, which are poorly screened by the excess ladder charges. There are two possible scenarios here, which cannot be distinguished in our experiments. One is based on current SCCO literature, where it is widely accepted that Sr-Ca substitution transfers electrons from ladders to the edge-sharing chains[6,24] where they tend to localize[40] and exert an attractive potential on the ladder holes. (This scenario can be viewed as a sort of excitonic formation between the particle-hole pair introduced by the charge transfer process.) Alternatively, Ca could be acquiring excess charges from the Sr sites, however, this is unlikely for two isovalent elements. Lastly, chemical doping in q-1D materials is often associated with structural distortions that lead to varied magnetic exchange couplings[41,42]. We tested

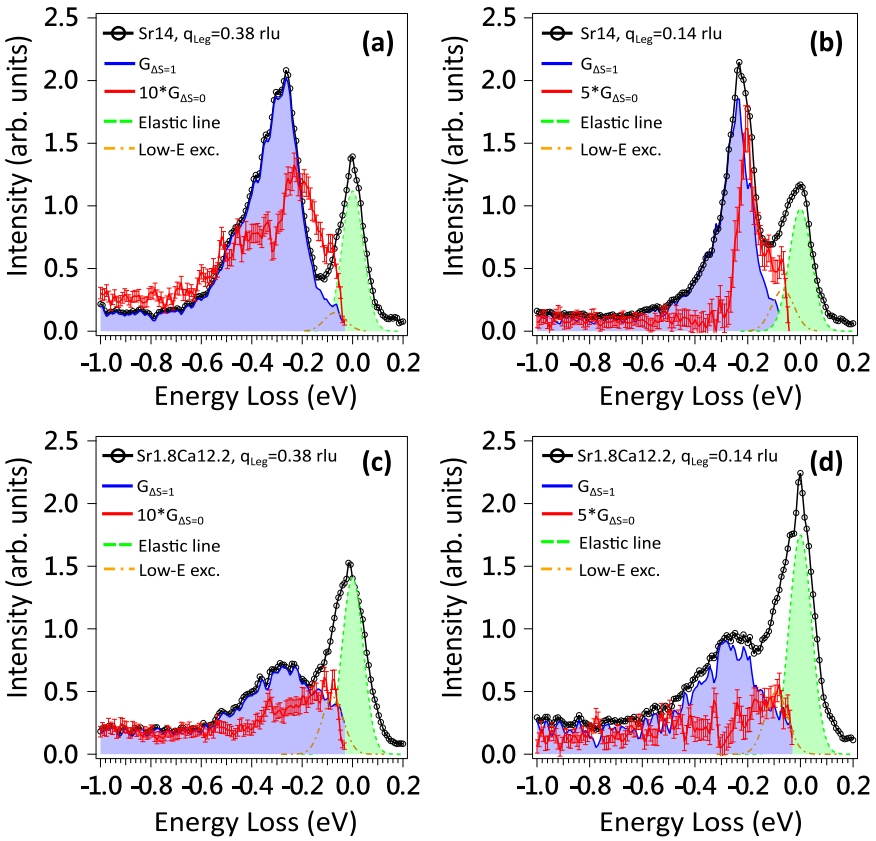

Fig. 4 Disentangled spin and charge dynamics by polarization-resolved RIXS. Cu L_3-edge RIXS spectra with $\Delta S = 1$ (blue-shadowed) and $\Delta S = 0$ (red line) channels disentangled for (**a**–**b**) Sr14 and (**c**–**d**) Sr1.8Ca12.2 taken at $q_{\mathrm{leg}} = 0.38$ rlu (**a**, **c**) and $q_{\mathrm{leg}} = 0.14$ rlu (**b**, **d**). Experimental data shown here are taken with π polarization in grazing emission geometry. We remind the reader that the RIXS intensity $I(\varepsilon, q)$ can be expressed as combination of $\Delta S = 1$ and $\Delta S = 0$ dynamical structure factors $G(\Delta S, \varepsilon, q, \omega)$ multiplied by form factors $F(\Delta S, \varepsilon, q)$ of the scattering processes[22,46,60].

the possibility of such a scenario and found it inconsistent with our estimated ladder-rung couplings in Sr1.8Ca12.2. (see Supplementary Fig. 14)

To examine the feasibility of the localization proposal, we modeled the unscreened off-ladder impurities by introducing an extended impurity potential with 12.5% coverage of ladder sites (see Supplementary Note 3). The on-site value of the potential was set to $V_{\mathrm{imp}} = 0.5\,U$ while the values on the neighboring sites up to next-nearest-neighbors was scaled as $\propto 1/r$, as sketched in the inset of Fig. 2f. The resulting simulated RIXS signal in the $\Delta S = 1$ channel after averaging over eight disorder configurations is shown in Fig. 2f. The downward dispersing spectral weight near zone center is suppressed, while the overall dispersion flattens close to the zone boundary. These modeled spectra are in closer agreement with the experiments and demonstrate that local impurities and charge localization are a plausible explanation for the flattened magnetic excitations. However, we also note that there remains a non-negligible difference between the theory and experiment at small momentum transfers. This may be due to the absence of RIXS dipole matrix elements, or the overall simplicity of our model. A third possibility could be finite size effects in our calculations. Due to the large computational time required by our DMRG simulations, we have found a compromise between the largest cluster size compatible with the nominal doping extracted from the XAS analysis (~11%), the highest coverage of impurities (up to 12.5%), disorder averaging (up to 8 configurations), and the largest attainable precision (see Supplementary Note 3). Nevertheless, our results suggest that other factors beyond simple charge doping such as localization need to be invoked for explaining the evolution of the magnetic RIXS response with increasing Ca content.

Polarization-resolved RIXS analysis

To gather additional support for our interpretation of localized holes in the ladders of Sr1.8Ca12.2, we performed a polarimetric analysis of the RIXS measurements to assess the character of charge and spin scattering in the low-energy excitations[33,43–45]. Here, we apply the method established in ref. [43] to disentangle $\Delta S = 1$ and $\Delta S = 0$ channels of the RIXS response, which was previously demonstrated for the two-spinon excitations of $CaCu_2O_3$. (see Supplementary Note 4) This approach is based on the idea that the RIXS intensity can be expressed as the product of a dynamical structure factor $G(\Delta S, \varepsilon, q, \omega)$ and a form factor $F(\Delta S, \varepsilon, q)$ such that $I(\varepsilon, q) = G(\Delta S, \varepsilon, q, \omega) F(\Delta S, \varepsilon, q)$[22,46]. Here, ω, ε (σ or π), and q are the energy loss, incident X-ray polarization, and momentum-transfer, respectively. By calculating the form factors $F(\Delta S, \varepsilon, q)$ for respective $\Delta S = 1$ and $\Delta S = 0$ scattering channels, we extract the spin-resolved structure factors $G(\Delta S, \varepsilon, q, \omega)$ from the measured $I(\varepsilon, q)$ in polarization-resolved RIXS experiments. In this work, we follow the single-ion picture in ref. [43] where the local spin-flip and charge scattering probabilities $P(\Delta S, \varepsilon, q)$ are used to approximate the form factors $F(\Delta S, \varepsilon, q)$.

Figure 4 compares the $\Delta S = 1$ and $\Delta S = 0$ signal for $q_{\mathrm{leg}} = 0.38$ and 0.14 rlu. We find that the $\Delta S = 1$ channel indeed provides the major contribution to the low-energy RIXS response for both Sr14 and Sr1.8Ca12.2, confirming a magnetic origin for these excitations. In Sr14 (Fig. 4a, b), the $\Delta S = 0$ scattering is dominated by a sharp mode at slightly reduced energy compared to the $\Delta S = 1$

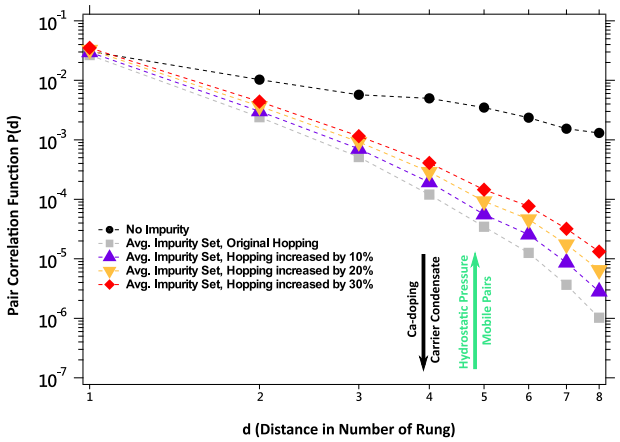

Fig. 5 Calculated pair correlations with Ca-doping and static pressure effects. Rung-singlet pair correlations plotted as a function of distance along the ladder-leg direction in logarithmic scale. For simplicity, the increasing hopping integral for simulating static pressure is uniform over the ladder cluster. The Hubbard repulsion and impurity potential V_{imp} are kept fixed in these calculations.

channel. Progress has recently been made in understanding the RIXS response in $\Delta S = 0$ channel of the ladder system, which indeed predicts a sharp bound two-triplon state in this channel[37,47]. Additionally, a broad component centered around 400–600 meV appears in this channel, which is more pronounced near the zone boundary, coinciding with the momentum region where the excitation profiles show a stronger high-energy tail (Fig. 2a). The energy scale of these excitations is comparable to the theoretically predicted charge and $\Delta S = 0$ multi-triplon excitations[11,37]. Additionally, these modes resemble the 500 meV peak in the $\Delta S = 0$ RIXS channel of 2D cuprates[48–51], while its nature and connection to ladder excitations remains an open question.

The $\Delta S = 0$ channel in Sr1.8Ca12.2, on the other hand, is essentially a structure-less background below −1 eV loss, as shown in Fig. 4c, d. Since these excitations arise from low-energy charge and $\Delta S = 0$ multi-triplon excitations, their suppression with Ca doping is consistent with localization. Previous theoretical studies on 2D $3d^9$ cuprates and ladders have demonstrated that the Cu L_3-edge RIXS signal is dominated by single spin-flip excitations, with additional intensity modulations induced by the dipole matrix elements[33]. At the same time, the leading contribution in the $\Delta S = 0$ channel of the doped system comes from charge (particle-hole) excitations[33,37]. With mobile carriers, the $\Delta S = 0$ response is dominated by the charge continuum with excitations extending to zero-energy[33,37]. Conversely, with localized charges, the charge excitations are gapped with weight transferred to higher-energy[33,37]. This behavior is also captured by the calculated modified dynamical charge structure factor that reflects the RIXS intensity in this scattering channel. (see Supplementary Fig. 15) We, therefore, conclude that the observed non-dispersive and damped magnetic excitations in Sr1.8Ca12.2 can be understood using a hole-immobilized ladder picture, despite an increased carrier density.

Superconducting correlations

We now explore the implications of our results for superconductivity in the Ca-rich samples. Here, we envision that the localized carriers with Sr-Ca substitution will be released as hydrostatic pressure is applied, eventually forming a superconducting condensate. We again model the effects of Ca doping by introducing the same random impurity configurations used to simulate the spectra discussed in the previous sections. We then assume that the primary effect of the hydrostatic pressure is to reduce the lattice bond distances, thus effectively increasing the hopping integrals while holding the impurity potentials fixed. (For simplicity, we assume that all hopping integrals increase uniformly in the ladders with pressure.) This procedure thus captures the competition between the localizing potentials introduced by Ca-doping and the increase of bandwidth introduced by pressure. We then compute the pair correlations (see methods) for the clean system and for the averaged impurity configurations with increased hopping, as shown in Fig. 5. Without impurities, we obtain a power-law dependence in the pair correlations, indicating strong pairing tendencies. The correlations are exponentially suppressed when we introduce the impurity potentials. As hydrostatic pressure is applied and the hopping increases, the pair correlations begin to recover the robust behavior of the clean system.

DISCUSSION

Our results have important consequences for understanding the starting condition from which the SC state in SCCO is established with high Ca content and elevated pressures. Despite the idealized assumptions of our model, our results imply that off-plane impurity potentials can significantly shape the low-energy magnetic and superconducting properties of the cuprate ladders. The ingredients of a complete theory must now reconcile the roles of Sr-Ca substitution, magnetic and charge fluctuations, and the observed localization in Ca-doped SCCO.

We believe that this issue should also be re-visited in 2D cuprates, where impurities in the charge reservoir layers are poorly screened. Noticeably, INS studies have revealed similar localized multi-magnon excitations in the $\Delta S = 1$ channel at ~130 meV in 2D superconducting cuprates. With elevated hole concentration, the excitation energy was interpreted as scaled with the pseudogap energy upon doping[52]. We connect this observation to our measured localized magnetic excitations because of a pseudogap-like feature ~100 meV observed in $x = 11$ SCCO samples using optical sepctroscopy[53]. Unfortunately, this mode could be obscured by our instrumental resolution of ~95 meV. To further elucidate the overall effects of Sr-Ca replacement in SCCO, we suggest future experiments using INS at high-pressure or higher-resolution RIXS for measuring momentum-resolved magnetic excitations. This will help to clarify the underlying electronic correlations connected to pairing in SCCO as well as the microscopic interactions of other competing electronic phases, e.g. pseudogap formation[53].

In summary, we have performed Cu L_3-edge RIXS measurements on the spin ladder in SCCO. We observed a crossover in the magnetic excitation spectrum from the collective 2 T excitations in Sr14 to a high-energy incoherent gapped magnetic excitations in Sr1.8Ca12.2. By comparing these with spectra evaluated using DMRG calculations on a model Hamiltonian, we conclude that the observed reorganization of the magnetic excitations reflects a tendency towards carrier-immobility in the Ca-doped system. This conclusion was supported by polarization-dependent RIXS measurements, where we extracted a clear suppression of the $\Delta S = 0$ channel from well-defined charge and multi-triplon excitations ($x = 0$) to a featureless background ($x = 12.2$). We further calculated the pair correlations, and our results indicated that (Sr,Ca) layer impurities could impact the low-energy properties of the ladder subsystem. Our work calls for future studies re-examining the role of off-plane impurities in 2D cuprates in the doped regime where superconductivity, pseudogap, as well as charge and spin orders compete. Finally, our results on localized excitations with Ca-doping could be useful to understand pair (pre-) formation in the pseudogap regime. On the other hand, our work gives valuable information on the dynamics of q-1D cuprate ladders, as well as their relationship with various competing electron-pairing hypotheses.

METHODS

RIXS experiment

Single crystals of $Sr_{14}Cu_{24}O_{41}$ (Sr14) and $Sr_{1.8}Ca_{12.2}Cu_{24}O_{41}$ (Sr1.8Ca12.2) were grown with the traveling-solvent floating zone method[54,55]. The samples were cut and polished to form the a-c plane, with the b-axis pointing out-of-plane. Subsequently, top-post cleavage was performed in-situ before all measurements in a vacuum pressure of better than 5×10^{-10} mbar. Cu L_3-edge RIXS and X-ray absorption spectroscopy (XAS) measurements were performed at the Advanced Resonant Spectroscopies (ADRESS) beamline at the Swiss Light Source (SLS), Paul Scherrer Institut[56–58]. The total energy resolution of the RIXS experiment was ~95 meV at the Cu L_3-edge (930 eV). The RIXS spectrometer was fixed at a scattering angle $2\theta = 130°$ while the experimental geometry was set such that the crystallographic b- and c-axis of the sample lay in the scattering plane (Fig. 1a). This geometry allows no momentum-transfer along the ladder rungs and selectively enhances the multi-triplon RIXS response with even-parity along $\mathbf{q} = (q_{\text{leg}}, q_{\text{rung}} = 0)$[23,59]. RIXS measurements were acquired with 15 min per spectrum, and normalized to the total spectral weight of the crystal-field excitations. XAS spectra were recorded in total fluorescence yield (TFY) mode. σ polarization was employed for the incident X-rays, unless specified otherwise. All measurements were taken at base temperature 20 K.

DMRG calculation

We use a single band Hubbard ladder with nearest neighbor hopping to model the system (see Supplementary Note 3). The lowest order contributions at the Cu L_3-edge are given by the dynamical spin structure factor $S(q, \omega)$, and a modified dynamical charge structure factor $\tilde{N}(q, \omega)$[33]. These structure factors are calculated as:

$$S(q,\omega) = \sum_{f,\sigma} \left| \langle f | S^z_{q,\sigma} | g \rangle \right|^2 \delta(E_f - E_g + \omega) \tag{1}$$

and

$$\tilde{N}(q,\omega) = \sum_{f,\sigma} \left| \langle f | \tilde{n}_{q,\sigma} | g \rangle \right|^2 \delta(E_f - E_g + \omega), \tag{2}$$

where

$$\tilde{n}_{q,\sigma} = n_{q,\sigma} - n_{q,\sigma} n_{q,\sigma'} \tag{3}$$

Here, q and ω are the net (1D) momentum and energy transfer to the system, σ is a spin index, g and f are the initial and final states of the scattering process, respectively, E_g and E_f are their respective energies, and $S^z_{q,\sigma}$ and $\tilde{n}_{q,\sigma}$ are the Fourier transforms of the local spin and charge operators, respectively. For Sr14, we use a 32×2 ladder cluster and keep up to $m = 1000$ states and a maximum truncation error of 10^{-7}. The artificial broadening parameter is set to $\eta = 47.5$ meV to match the experimental resolution. For Sr1.8Ca12.2, we use a 16×2 ladder with the same $m = 1000$ states and artificial broadening parameter η as was used for Sr14. The maximum truncation error is reduced to 10^{-8}. The impurity potentials $V_{\text{imp}} = 0.5\,U$ are introduced at four randomly chosen sites in the ladders and extended to nearest neighbors with appropriate rescaling of strength (see Supplementary Note 3 and Fig. 9). To understand the implications of hole localization in the pairing tendencies exhibited by the carriers in the ladder, we further calculate the averaged rung singlet pair correlation function $P(d)$ as a function of distance d

$$P(d) = \frac{1}{L-d} \sum_{j=1}^{L-d} \left\langle \Delta_j^\dagger \Delta_{j+d} \right\rangle, \tag{4}$$

where $\Delta_i^\dagger$ is defined[2] as

$$\frac{1}{\sqrt{2}} \left(c^\dagger_{i,0,\uparrow} c^\dagger_{i,1,\downarrow} - c^\dagger_{i,0,\downarrow} c^\dagger_{i,1,\uparrow} \right). \tag{5}$$

DATA AVAILABILITY

All the data used in the present manuscript and Supplementary Information can be found at https://doi.org/10.5281/zenodo.6914223.

CODE AVAILABILITY

All numerical results were computed using the DMRG++ computer program available at https://github.com/g1257/dmrgpp.git. The code used to perform the theory simulations can be found at https://doi.org/10.5281/zenodo.6914223.

Received: 9 April 2022; Accepted: 30 August 2022;
Published online: 15 September 2022

REFERENCES

1. Eschrig, M. The effect of collective spin-1 excitations on electronic spectra in high-Tc superconductors. *Adv. Phys.* **55**, 47–183 (2006).
2. Nocera, A., Patel, N. D., Dagotto, E. & Alvarez, G. Signatures of pairing in the magnetic excitation spectrum of strongly correlated two-leg ladders. *Phys. Rev. B* **96**, 205120 (2017).
3. Dagotto, E., Riera, J. & Scalapino, D. Superconductivity in ladders and coupled planes. *Phys. Rev. B* **45**, 5744–5747 (1992).
4. Rice, T. M., Gopalan, S. & Sigrist, M. Superconductivity, spin gaps and Luttinger liquids in a class of cuprates. *Europhys. Lett.* **23**, 445–449 (1993).
5. Dagotto, E. & Rice, T. M. Surprises on the way from one- to two-dimensional quantum magnets: The ladder materials. *Science* **271**, 618–623 (1996).
6. Motoyama, N., Osafune, T., Kakeshita, T., Eisaki, H. & Uchida, S. Effect of Ca substitution and pressure on the transport and magnetic properties with doped two-leg Cu-O ladders. *Phys. Rev. B* **55**, R3386–R3389 (1997).
7. Eccleston, R. S. et al. Spin dynamics of the spin-ladder dimer-chain material $Sr_{14}Cu_{24}O_{41}$. *Phys. Rev. Lett.* **81**, 1702–1705 (1998).
8. Uehara, M. et al. Superconductivity in the ladder material $Sr_{0.4}Ca_{13.6}Cu_{24}O_{41.84}$. *J. Phys. Soc. Jpn.* **65**, 2764–2767 (1996).
9. Nagata, T. et al. Pressure-induced dimensional crossover and superconductivity in the hole-doped two-leg ladder compound $Sr_{14-x}Ca_xCu_{24}O_{41}$. *Phys. Rev. Lett.* **81**, 1090–1093 (1998).
10. Nakanishi, T. et al. High-pressure transport properties of the superconducting spin-ladder system $Sr_{14-x}Ca_xCu_{24}O_{41}$. *J. Phys. Soc. Jpn.* **67**, 2408–2414 (1998).
11. Schmidt, K. P. & Uhrig, G. S. Spectral properties of magnetic excitations in cuprate two-leg ladder systems. *Mod. Phys. Lett. B* **19**, 1179–1205 (2005).
12. Notbohm, S. et al. One- and two-triplon spectra of a cuprate ladder. *Phys. Rev. Lett.* **98**, 027403 (2007).
13. Vojta, M. & Ulbricht, T. Magnetic excitations in a bond-centered stripe phase: Spin waves far from the semiclassical limit. *Phys. Rev. Lett.* **93**, 127002 (2004).
14. Tranquada, J. M. et al. Quantum magnetic excitations from stripes in copper oxide superconductors. *Nature* **429**, 534–538 (2004).
15. Greiter, M. & Schmidt, H. Evidence for site-centered stripes from magnetic excitations in cuprate superconductors. *Phys. Rev. B* **82**, 144512 (2010).
16. Katano, S., Nagata, T., Akimitsu, J., Nishi, M. & Kakurai, K. Spin gap in the hole-doped spin ladder system $(Sr_{2.5}Ca_{11.5})Cu_{24}O_{41}$: Neutron inelastic scattering study. *Phys. Rev. Lett.* **82**, 636–639 (1999).
17. Deng, G. et al. Spin-gap evolution upon Ca doping in the spin-ladder series $Sr_{14-x}Ca_xCu_{24}O_{41}$ studied by inelastic neutron scattering. *Phys. Rev. B* **88**, 014504 (2013).
18. Kumagai, K. I., Tsuji, S., Kato, M. & Koike, Y. NMR study of carrier doping effects on spin gaps in the spin ladder $Sr_{14-x}A_xCu_{24}O_{41}$ (A = Ca, Y, and La). *Phys. Rev. Lett.* **78**, 1992–1995 (1997).
19. Magishi, K., Matsumoto, S., Kitaoka, Y., Ishida, K. & Asayama, K. Spin gap and dynamics in comprising hole-doped two-leg spin ladders: Cu NMR study on single crystals. *Phys. Rev. B* **57**, 11533–11544 (1998).
20. Mayaffre, H. et al. Absence of a spin gap in the superconducting ladder compound $Sr_2Ca_{12}Cu_{24}O_{41}$. *Science* **279**, 345–348 (1998).
21. Ament, L. J. P., van Veenendaal, M., Devereaux, T. P., Hill, J. P. & van den Brink, J. Resonant inelastic x-ray scattering studies of elementary excitations. *Rev. Mod. Phys.* **83**, 705–767 (2011).
22. Ament, L. J. P., Ghiringhelli, G., Sala, M. M., Braicovich, L. & van den Brink, J. Theoretical demonstration of how the dispersion of magnetic excitations in cuprate compounds can be determined using resonant inelastic X-ray scattering. *Phys. Rev. Lett.* **103**, 117003 (2009).
23. Schlappa, J. et al. Collective magnetic excitations in the spin ladder $Sr_{14}Cu_{24}O_{41}$ measured using high-resolution resonant inelastic x-ray scattering. *Phys. Rev. Lett.* **103**, 047401 (2009).

24. Osafune, T., Motoyama, N., Eisaki, H. & Uchida, S. Optical study of the $Sr_{14-x}Ca_xCu_{24}O_{41}$ system: Evidence for hole-doped Cu_2O_3 ladders. *Phys. Rev. Lett.* **78**, 1980–1983 (1997).
25. Kato, M., Shiota, K., Adachi, T. & Koike, Y. Metal-insulator transition and spin gap in the spin-ladder cuprate $Sr_{14-x}A_xCu_{24}O_{41}$ (A = Ca, Ba, Y, La). *Czechoslov. J. Phys.* **46**, 2701–2702 (1996).
26. Mizuno, Y., Maekawa, S., Tohyama, T. & Maekawa, S. Electronic states of doped spin ladders $(Sr,Ca)_{14}Cu_{24}O_{41}$. *J. Phys. Soc. Jpn.* **66**, 937–940 (1997).
27. Deng, G. et al. Structural evolution of one-dimensional spin-ladder compounds $Sr_{14-x}Ca_xCu_{24}O_{41}$ with Ca doping and related evidence of hole redistribution. *Phys. Rev. B* **84**, 144111 (2011).
28. Ilakovac, V. et al. Hole depletion of ladders in $Sr_{14}Cu_{24}O_{41}$ induced by correlation effects. *Phys. Rev. B* **85**, 075108 (2012).
29. Nücker, N. et al. Hole distribution in $(Sr,Ca,Y,La)_{14}Cu_{24}O_{41}$ ladder compounds studied by x-ray absorption spectroscopy. *Phys. Rev. B* **62**, 14384–14392 (2000).
30. Rusydi, A. et al. Relationship between hole density and charge-ordering wave vector in Sr_{14-x} $Ca_xCu_{24}O_{41}$. *Phys. Rev. B* **75**, 104510 (2007).
31. Kabasawa, E. et al. Hole distribution in $(Sr,Ca,Y,La)_{14}Cu_{24}O_{41}$ compounds studied by x-ray absorption and emission spectroscopy. *J. Phys. Soc. Jpn.* **77**, 034704 (2008).
32. van den Brink, J. & van Veenendaal, M. Theory of indirect resonant inelastic X-ray scattering. *J. Phys. Chem. Solids* **66**, 2145–2149 (2005).
33. Jia, C., Wohlfeld, K., Wang, Y., Moritz, B. & Devereaux, T. P. Using RIXS to uncover elementary charge and spin excitations. *Phys. Rev. X* **6**, 021020 (2016).
34. Kumar, U. et al. Unraveling higher-order contributions to spin excitations probed using resonant inelastic x-ray scattering. *Phys. Rev. B* **106**, L060406 (2022).
35. White, S. R. Density matrix formulation for quantum renormalization groups. *Phys. Rev. Lett.* **69**, 2863–2866 (1992).
36. White, S. R. Density-matrix algorithms for quantum renormalization groups. *Phys. Rev. B* **48**, 10345–10356 (1993).
37. Kumar, U., Nocera, A., Dagotto, E. & Johnston, S. Theoretical study of the spin and charge dynamics of two-leg ladders as probed by resonant inelastic x-ray scattering. *Phys. Rev. B* **99**, 205130 (2019).
38. Tacon, M. L. et al. Intense paramagnon excitations in a large family of high-temperature superconductors. *Nat. Phys.* **7**, 725–730 (2011).
39. Dean, M. P. M. et al. Persistence of magnetic excitations in $La_{2-x}Sr_xCuO_4$ from the undoped insulator to the heavily overdoped non-superconducting metal. *Nat. Mater.* **12**, 1019–1023 (2013).
40. Drechsler, S. L. et al. Intersite Coulomb interactions in edge-shared CuO_2 chains: Optics and EELS. *Phys. C. Supercond. its Appl.* **470**, S84–S85 (2010).
41. Hammerath, F. et al. Spin gap in the zigzag spin-1/2 chain cuprate $Sr_{0.9}Ca_{0.1}CuO_2$. *Phys. Rev. Lett.* **107**, 017203 (2011).
42. Hammerath, F. et al. Spin gap in the single spin-1/2 chain cuprate $Sr_{1.9}Ca_{0.1}CuO_3$. *Phys. Rev. B* **89**, 184410 (2014).
43. Bisogni, V. et al. Femtosecond dynamics of momentum-dependent magnetic excitations from resonant inelastic x-ray scattering in $CaCu_2O_3$. *Phys. Rev. Lett.* **112**, 147401 (2014).
44. Hepting, M. et al. Three-dimensional collective charge excitations in electron-doped copper oxide superconductors. *Nature* **563**, 374–378 (2018).
45. Fumagalli, R. et al. Polarization-resolved Cu L_3-edge resonant inelastic X-ray scattering of orbital and spin excitations in $NdBa_2Cu_3O_{7-\delta}$. *Phys. Rev. B* **99**, 134517 (2019).
46. Haverkort, M. W. Theory of resonant inelastic x-ray scattering by collective magnetic excitations. *Phys. Rev. Lett.* **105**, 167404 (2010).
47. Schmiedinghoff, G., Müller, L., Kumar, U., Uhrig, G. S. & Fauseweh, B. Three-body bound states in antiferromagnetic spin ladders. *Commun. Phys.* **5**, 218 (2022).
48. Hill, J. P. et al. Observation of a 500 meV collective mode in $La_{2-x}Sr_xCuO_4$ and Nd_2CuO_4 using resonant inelastic X-ray scattering. *Phys. Rev. Lett.* **100**, 097001 (2008).
49. Ellis, D. S. et al. Magnetic nature of the 500 meV peak in $La_{2-x}Sr_xCuO_4$ observed with resonant inelastic x-ray scattering at the Cu K-edge. *Phys. Rev. B* **81**, 085124 (2010).
50. Bisogni, V. et al. Bimagnon studies in cuprates with resonant inelastic x-ray scattering at the O K edge. I. Assessment on La_2CuO_4 and comparison with the excitation at Cu L_3 and Cu K edges. *Phys. Rev. B* **85**, 214527 (2012).
51. Bisogni, V. et al. Bimagnon studies in cuprates with resonant inelastic x-ray scattering at the O K edge. II. Doping effect in $La_{2-x}Sr_xCuO_4$. *Phys. Rev. B* **85**, 214528 (2012).
52. Stock, C. et al. Effect of the pseudogap on suppressing high energy inelastic neutron scattering in superconducting $YBa_2Cu_3O_{6.5}$. *Phys. Rev. B* **82**, 174505 (2010).
53. Osafune, T., Motoyama, N., Eisaki, H., Uchida, S. & Tajima, S. Pseudogap and collective mode in the optical conductivity spectra of hole-doped ladders $Sr_{14-x}Ca_xCu_{24}O_{41}$. *Phys. Rev. Lett.* **82**, 1313–1316 (1999).
54. Deng, G. et al. High oxygen pressure single crystal growth of highly Ca-doped spin ladder compound $Sr_{14-x}Ca_xCu_{24}O_{41}$ (x > 12). *J. Cryst. Growth* **327**, 182–188 (2011).
55. Bag, R., Karmakar, K. & Singh, S. Travelling-solvent floating-zone growth of the dilutely Co-doped spin-ladder compound $Sr_{14}(Cu, Co)_{24}O_{41}$. *J. Cryst. Growth* **458**, 16–26 (2017).
56. Ghiringhelli, G. et al. SAXES, a high resolution spectrometer for resonant x-ray emission in the 400–1600 eV energy range. *Rev. Sci. Instrum.* **77**, 113108 (2006).
57. Strocov, V. N. et al. High-resolution soft X-ray beamline ADRESS at the Swiss Light Source for resonant inelastic X-ray scattering and angle-resolved photoelectron spectroscopies. *J. Synchrotron Radiat.* **17**, 631–643 (2010).
58. Strocov, V. N., Schmitt, T., Flechsig, U., Patthey, L. & Chiuzbăian, G. S. Numerical optimization of spherical variable-line-spacing grating X-ray spectrometers. *J. Synchrotron Radiat.* **18**, 134–142 (2011).
59. Nagao, T. & Igarashi, J. I. Theory of L-edge resonant inelastic x-ray scattering for magnetic excitations in two-leg spin ladders. *Phys. Rev. B* **85**, 224436 (2012).
60. Braicovich, L. et al. Momentum and polarization dependence of single-magnon spectral weight for Cu L_3-edge resonant inelastic x-ray scattering from layered cuprates. *Phys. Rev. B* **81**, 174533 (2010).

ACKNOWLEDGEMENTS

The experiments have been performed at the ADRESS beamline of the Swiss Light Source at the Paul Scherrer Institut (PSI). The work at PSI is supported by the Swiss National Science Foundation through project no. 200021_178867, and the Sinergia network Mott Physics Beyond the Heisenberg Model (MPBH) (SNSF Research Grants CRSII2_160765/1 and CRSII2_141962). T.C.A. acknowledges funding from the European Union's Horizon 2020 research and innovation programme under the Marie Skłodowska-Curie grant agreement No. 701647 (PSI-FELLOW-II-3i program). Y.T. and T.S. would like to thank V. Bisogni for valuable discussions. A.N. acknowledges, in part, funding from the Max Planck-UBC-UTokyo Center for Quantum Materials and the Canada First Research Excellence Fund, Quantum Materials and Future Technologies Program. J.T. and S.J. are supported by the National Science Foundation under Grant No. DMR-1842056. This work used computational resources supported by the University of Tennessee and Oak Ridge National Laboratory Joint Institute for Computational Sciences, and computational resources and services provided by Advanced Research Computing at the University of British Columbia.

AUTHOR CONTRIBUTIONS

Y.T. and T.S. designed the experiment; Y.T., W.Z., E.P., T.C.A. and T.S. performed the experiment with the assistance of V.N.S., J.T., A.N. and S.J. performed the DMRG calculations with the assistance of U.K., R.B. and S.S. prepared and characterized the Sr14 single crystal samples; P.P, G.D. and E.K. prepared and characterized the Sr1.8Ca12.2 single crystal samples; Y.T. performed data analysis in discussion with J.T., A.N., H.M.R., S.J. and T.S., S.J. and T.S. were responsible for project management; Y.T., J.T., A.N. S.J. and T.S. wrote the paper together with input from all other authors.

COMPETING INTERESTS

The authors declare no competing interests.

ADDITIONAL INFORMATION

Supplementary information The online version contains supplementary material available at https://doi.org/10.1038/s41535-022-00502-1.

Correspondence and requests for materials should be addressed to Y. Tseng, S. Johnston or T. Schmitt.

Reprints and permission information is available at http://www.nature.com/reprints

Publisher's note Springer Nature remains neutral with regard to jurisdictional claims in published maps and institutional affiliations.